Available online at www.sciencedirect.com

ScienceDirect

Procedia Structural Integrity 44 (2023) 1554–1561

Structural Integrity Procedia

www.elsevier.com/locate/procedia

XIX ANIDIS Conference, Seismic Engineering in Italy

A simplified procedure to assess uncertainties in the estimation of the rigid motion of isolated buildings based on InSAR monitoring

Elisa Bassoli[a], Francesca Grassi[a], Ghita Eslami Varzaneh[a], Federico Ponsi[b], Francesco Mancini[a], Loris Vincenzi[a]*

[a] *University of Modena and Reggio Emilia, Department of Engineering Enzo Ferrari, Via P. Vivarelli 10, Modena 41125, Italy*
[b] *University of Bologna, Department of Civil, Chemical, Environmental, and Materials Engineering, Viale Risorgimento 2, Bologna 40126, Italy*

Abstract

This paper proposes a method to monitor the rigid motion of isolated buildings based on DInSAR technology. The satellite monitoring of isolated buildings is made possible by both the availability of high resolution data thanks to the current generation of SAR constellations and the combination of measurements from dual orbits. However, to assess whether the accuracy of the estimated motion is enough for structural monitoring purposes, the uncertainties of the estimated motion components need to be evaluated as well. To this aim, an analytical procedure to evaluate the estimated parameter uncertainties is also proposed. The proposed procedure is based on the simplifying assumption that the rigid motion components are independent of each other. The performance of the presented analytical procedure is investigated by comparing the analytical uncertainties to those obtained from numerical simulations, performed accounting for the uncertainties affecting SAR data. These last are related to the measurement uncertainties and errors in the positioning of the permanent scatterers.

Keywords: Multi-temporal DInSAR; Persistent Scatterer Interferometry; structural monitoring; 3D rigid motion; motion parameters uncertainties

1. Introduction

Differential Interferometric Synthetic Aperture Radar (DInSAR) is a satellite-based remote sensing technique, whose multi-temporal use has been adopted to monitor large scale displacements such as subsidence, landslides,

* Corresponding author. Tel.: +390592056213; fax: +390592056126.
E-mail address: loris.vincenzi@unimore.it

10.1016/j.prostr.2023.01.199

earthquakes, since the 1980s (Barreca et al., 2014; Calò et al., 2014). Its application at (infra)structure scale is instead quite recent, made possible by the improved imaging capability of the current generation of SAR constellations. Despite the relative novelty, several investigations about Structural Health Monitoring (SHM) based on SAR data have been conducted to date (Bianchini et al., 2015; Cavalagli et al., 2019; Milillo et al., 2019; Noviello et al., 2020; Reale et al., 2011; Talledo et al., 2022). However, an automated procedure to reconstruct building motion and analyses regarding the uncertainties of achieved results are still missing in the literature.

SAR techniques are basically affected by two error sources: radar satellite displacement measurements and Persistent Scatterer (PS) positioning. The entity of such errors, which depends on the chosen constellation, affects the accuracy of the estimated building motion. Although the displacement uncertainty along the Line of Sight (LOS) direction is known, the incidence of PS positioning errors is still not as familiar. Moreover, the propagation of errors into the resulting building motion has not yet been explored. To fill this gap, the paper is aimed at providing simplified analytical definitions of such unknowns. Their use would allow to understand in advance whether the DInSAR technique is suitable to obtain the accuracy needed. Indeed, knowing the building plan size, the proposed procedure is able to assess a priori (i.e. without still having any SAR data) if the reliability of the potential result is enough to detect the expected motion.

Firstly, the building motion arising from the use of SAR data is introduced in Section 2. The building is supposed to be isolated and subject to rigid movements. Then, the propagation of errors from SAR data to the resulting building motion is investigated in Section 3. In this context, rigid motion uncertainties (due to displacement measurement and PS positioning errors) are addressed. The problem is set in the generic case, but analytical formulae are developed in the simplified case of motion components with uncorrelated uncertainties and building with flat roof. Afterwards, numerical simulations on a rectangular isolated building are performed, as illustrated in Section 4. Numerical simulations are used to validate the reliability of the aforementioned analytical expressions, as well as to characterize the reliability of the DInSAR approach to monitor the structural behavior. Finally, achievements, limitations and future perspectives are discussed in Section 5.

2. Isolated building 3D rigid motion

In this section, the procedure to reconstruct the rigid motion of an isolated building is presented. To evaluate the 3D rigid motion of isolated buildings, SAR measurements acquired from both ascending and descending satellite orbits are required. SAR data collected along the two orbits are not acquired at the same time, and PSs might be in different positions due to a non-uniform signal reflection. However, if mean annual values of displacements are considered, a perfect time correspondence of data is not needed. Besides, the lack of spatial correlation among the two orbits becomes irrelevant when dealing with a rigid motion, implying that ascending and descending PSs need not to be co-located. The adopted reference system is shown in Fig. 1, with x, y and z representing the west-east, north-south and vertical directions, respectively. Assuming clockwise rotations as positive, the displacement of a generic building point i relatively to G (the point on the ground corresponding to the building center of gravity) can be expressed as:

$$\begin{cases} v_{x,i} = v_{x,\mathrm{G}} + \phi_y \cdot D_{z,i} - \phi_z \cdot D_{y,i} \\ v_{y,i} = v_{y,\mathrm{G}} - \phi_x \cdot D_{z,i} + \phi_z \cdot D_{x,i} \\ v_{z,i} = v_{z,\mathrm{G}} + \phi_x \cdot D_{y,i} - \phi_y \cdot D_{x,i} \end{cases} \tag{1}$$

where $v_{x,G}$, $v_{y,G}$ and $v_{z,G}$ are the displacements of point G along x, y and z , $v_{x,i}$, $v_{y,i}$ and $v_{z,i}$ are the displacements of point i along the same directions, ϕ_x, ϕ_y and ϕ_z are the rotations around the three axes, $D_{x,i}$, $D_{y,i}$ and $D_{z,i}$ are the i to G distances in the three directions. Actually, SAR data do not provide the displacements of the i-th PS along the reference axes but along ascending and descending LOS directions, referred to as $d_{a,i}$ and $d_{d,i}$. Measured displacements can be written as functions of the x-y-z displacement components as:

$$\begin{cases} d_{a,i} = -v_{x,i} \cdot \cos\alpha_a + v_{z,i} \cdot \sin\alpha_a \\ d_{d,i} = +v_{x,i} \cdot \cos\alpha_d + v_{z,i} \cdot \sin\alpha_d \end{cases} \tag{2}$$

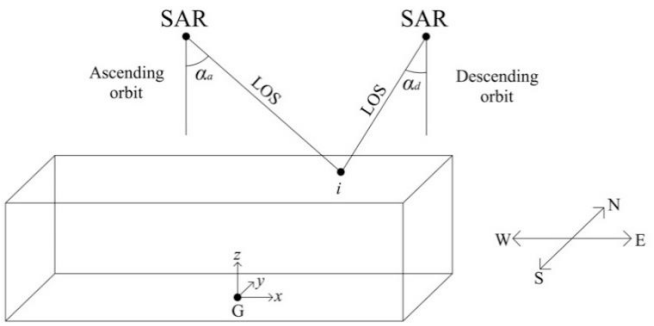

Fig. 1. Reference system and acquisition geometry of ascending and descending orbits.

where α_a and α_d are the ascending and descending satellite orbit incidence angles, respectively. Eq. (2) implies that the *y* displacement component cannot be reliably estimated by the procedure, due to the limited sensitivity of SAR displacement measurements along the north-south direction. Considering *n* and *m* measurements for ascending and descending orbits, respectively, the combination of Eq. (1) and Eq. (2) leads to the following matrix formulation:

$$\begin{bmatrix} d_{a,1} \\ \vdots \\ d_{a,n} \\ d_{d,1} \\ \vdots \\ d_{d,m} \end{bmatrix} = \begin{bmatrix} -\sin\alpha_a & \cos\alpha_a & D_{y,1}\cdot\cos\alpha_a & \left(-D_{z,1}\cdot\sin\alpha_a - D_{x,1}\cdot\cos\alpha_a\right) & D_{y,1}\cdot\sin\alpha_a \\ \vdots & \vdots & \vdots & \vdots & \vdots \\ -\sin\alpha_a & \cos\alpha_a & D_{y,n}\cdot\cos\alpha_a & \left(-D_{z,n}\cdot\sin\alpha_a - D_{x,n}\cdot\cos\alpha_a\right) & D_{y,n}\cdot\sin\alpha_a \\ \sin\alpha_d & \cos\alpha_d & D_{y,1}\cdot\cos\alpha_d & \left(D_{z,1}\cdot\sin\alpha_d - D_{x,1}\cdot\cos\alpha_d\right) & -D_{y,1}\cdot\sin\alpha_d \\ \vdots & \vdots & \vdots & \vdots & \vdots \\ \sin\alpha_d & \cos\alpha_d & D_{y,m}\cdot\cos\alpha_d & \left(D_{z,m}\cdot\sin\alpha_d - D_{x,m}\cdot\cos\alpha_d\right) & -D_{y,m}\cdot\sin\alpha_d \end{bmatrix} \begin{bmatrix} v_{x,G} \\ v_{z,G} \\ \phi_x \\ \phi_y \\ \phi_z \end{bmatrix} \tag{3}$$

whose compact form is here presented as $\mathbf{H}=\mathbf{Z}\,\boldsymbol{\theta}$, where $\mathbf{H}$ is a $(n+m)$-by-1 vector collecting the SAR displacement measurements along the two LOSs, $\mathbf{Z}$ is a $(n+m)$-by-5 matrix whose terms are related to PS positions and satellite acquisition geometries (i.e. incidence angles), and $\boldsymbol{\theta}$ is a 5-by-1 vector representing the five rigid motion components. It is worth highlighting that *n* and *m*, i.e. the PSs identified from ascending and descending orbits, are typically different in quantity and location. Optimal values of $\boldsymbol{\theta}$ are derived through the least square method, whose aim is to find the vector $\boldsymbol{\theta}$ that best fits the available measurements:

$$\boldsymbol{\theta} = (\mathbf{Z}^T\mathbf{Z})^{-1}\mathbf{Z}^T\mathbf{H} = \mathbf{B}\,\mathbf{H} \tag{4}$$

where $\mathbf{B}$ is a 5-by-$(n+m)$ matrix introduced for clarification purposes.

3. Analytical estimation of uncertainties in results

This section is aimed at analytically defining the effect of displacement measurement and PS positioning errors into the building rigid motion estimation, ruled by Eq. (4). Uncertainties due to the two sources of error are evaluated separately, and the law of propagation of uncertainties is used to derive the total variance. The analytical estimation of the covariance matrix of the rigid motion components due to measurement errors $\boldsymbol{\Sigma}_M(\boldsymbol{\theta})$ and that due to positioning errors $\boldsymbol{\Sigma}_P(\boldsymbol{\theta})$ are presented in Section 3.1 and Section 3.2. First of all, matrix expressions of general validity are derived. To ensure simplicity, the uncertainties of rigid motion components are then assumed to be uncorrelated, implying diagonal $\boldsymbol{\Sigma}_M(\boldsymbol{\theta})$ and $\boldsymbol{\Sigma}_P(\boldsymbol{\theta})$ matrices (the validity of such hypothesis is discussed in Section 5). The hypotheses of flat roof and uniformly distributed PSs are also introduced. The procedure might be further generalized to account for different PS heights, at the expense of the expression simpleness.

3.1. Displacement measurement errors

Eq. (4) implies that the covariance matrix of the rigid motion $\boldsymbol{\Sigma}_M(\boldsymbol{\theta})$ is proportional to that of the displacement measurements $\boldsymbol{\Sigma}(\mathbf{H})$:

$$\boldsymbol{\Sigma}_M(\boldsymbol{\theta}) = \mathbf{B}\,\boldsymbol{\Sigma}(\mathbf{H})\mathbf{B}^T \tag{5}$$

Indeed, matrix **B** is composed of terms depending on PS positions and satellite acquisition geometries, which are not affected by the displacement measurement uncertainty. The $(n+m)$-by-$(n+m)$ matrix $\boldsymbol{\Sigma}(\mathbf{H})$ is diagonal (as diverse displacement measurements are not subjected to any correlation), with all diagonal terms equal to the SAR measuring accuracy σ_H^2 . As stated above, the latter depends on the satellite constellation (e.g. σ_H is about 1-2 mm/year when dealing with COSMO-SkyMed data). It follows that:

$$\boldsymbol{\Sigma}_M(\boldsymbol{\theta}) = \sigma_H^2\mathbf{B}\,\mathbf{B}^T = \sigma_H^2\left[\left(\mathbf{Z}^T\mathbf{Z}\right)^{-1}\mathbf{Z}^T\right]\left[\left(\mathbf{Z}^T\mathbf{Z}\right)^{-1}\mathbf{Z}^T\right]^T = \sigma_H^2\left(\mathbf{Z}^T\mathbf{Z}\right)^{-1} \tag{6}$$

In conclusion, the rigid motion covariance $\boldsymbol{\Sigma}_M(\boldsymbol{\theta})$ is strictly related to σ_H^2 and depends on location and quantity of PSs through matrix **Z**. If the PS coordinates are known, **Z** can be simply derived and, in turn, also $\boldsymbol{\Sigma}_M(\boldsymbol{\theta})$. However, the aim of this paper is to provide a simple estimation of the result uncertainties in advance, before having any SAR data. Thus Eq. (6) is to be further processed, in order to remove the dependence on the PS positions from the $\boldsymbol{\Sigma}_M(\boldsymbol{\theta})$ definition. To simply approach the issue, the five rigid motion components are separately treated (i.e. $\boldsymbol{\Sigma}_M(\boldsymbol{\theta})$ is supposed to be diagonal). Considering only the horizontal displacement $v_{x,\mathrm{G}}$ without any other motion component, matrices **H** and **Z** become:

$$\mathbf{H} = \mathbf{Z}\cdot v_{x,G} \quad \text{with} \quad \mathbf{Z} = \left[-\sin\alpha_a \;\; \ldots \;\; -\sin\alpha_a \;\; \sin\alpha_d \;\; \ldots \;\; \sin\alpha_d\right]^T \tag{7}$$

Substituting Eq. (7) into Eq. (6), the reliability of the DInSAR technique on horizontal displacements reads:

$$\sigma_M^2\left(v_{x,G}\right) = \sigma_H^2\left(\mathbf{Z}^T\mathbf{Z}\right)^{-1} = \sigma_H^2\left(\sum_{i=1}^{n}\sin^2\alpha_a + \sum_{j=1}^{m}\sin^2\alpha_d\right)^{-1} = \frac{\sigma_H^2}{n\sin^2\alpha_a + m\sin^2\alpha_d} \tag{8}$$

depending on the number of PSs (i.e. n and m) but not on their positions. Similar conclusions can be drawn when the only vertical displacement component $v_{z,\mathrm{G}}$ is accounted for, with resulting variance equal to:

$$\sigma_M^2\left(v_{z,G}\right) = \frac{\sigma_H^2}{n\cos^2\alpha_a + m\cos^2\alpha_d} \tag{9}$$

The three rotation components ϕ_x, ϕ_y and ϕ_z are, separately, subjected to similar treatment. However, contrary to what happens on displacements $v_{x,\mathrm{G}}$ and $v_{z,\mathrm{G}}$, **Z** is no longer independent of the PS positions when a rotation is concerned. For instance, the estimated uncertainty of rotation ϕ_x reads:

$$\sigma_M^2\left(\phi_x\right) = \sigma_H^2\left(\cos^2\alpha_a\sum_{i=1}^{n}D_{y,i}^2 + \cos^2\alpha_d\sum_{j=1}^{m}D_{y,j}^2\right)^{-1} \tag{10}$$

To solve this, PSs are assumed to: (i) be uniformly distributed along the roof surface, and (ii) have all the same height. As a consequence, the following simplifications can be made:

$$\sum_{i=1}^{n} D_{x,i} = 0; \quad \sum_{j=1}^{m} D_{x,j} = 0; \quad \sum_{i=1}^{n} D_{y,i} = 0; \quad \sum_{j=1}^{m} D_{y,j} = 0; \quad \sum_{i=1}^{n} D_{z,i} = nD_z; \quad \sum_{j=1}^{m} D_{z,j} = mD_z; \tag{11}$$

$$\sum_{i=1}^{n} D_{x,i}^2 = n\rho_y^2; \quad \sum_{i=1}^{n} D_{y,i}^2 = n\rho_x^2; \quad \sum_{j=1}^{m} D_{x,j}^2 = m\rho_y^2; \quad \sum_{j=1}^{m} D_{y,j}^2 = m\rho_x^2; \tag{12}$$

where ρ_x and ρ_y are the radius of gyration of the building plan. These assumptions result in the following variances:

$$\sigma_M^2(\phi_x) = \frac{\sigma_H^2}{\rho_x^2\left(n\cos^2\alpha_a + m\cos^2\alpha_d\right)}; \quad \sigma_M^2(\phi_z) = \frac{\sigma_H^2}{\rho_x^2\left(n\sin^2\alpha_a + m\sin^2\alpha_d\right)} \tag{13}$$

$$\sigma_M^2(\phi_y) = \frac{\sigma_H^2}{D_z^2\left(n\sin^2\alpha_a + m\sin^2\alpha_d\right) + \rho_y^2\left(n\cos^2\alpha_a + m\cos^2\alpha_d\right)} \tag{14}$$

As regards the rotations around x and z axes, variances of DInSAR results are inversely related to the building extension in north-south direction. Note that a more extended plan dimension is also associated with a greater number of PSs, which produces an even more limited variance σ_M^2. On the other hand, the variance of the rotation around y is inversely proportional to D_z^2. The dependence from the latter means that, as expected, an increased building height entails a more accurate estimation of y rotations.

3.2. Persistent scatterer positioning errors

The propagation error theory applied to Eq. (4) allows to calculate the effect of PS positioning uncertainties $\mathbf{\Sigma(D)}$ on the rigid motion uncertainty $\mathbf{\Sigma}_P(\boldsymbol{\theta})$:

$$\mathbf{\Sigma}_P(\boldsymbol{\theta}) = \mathbf{J}\cdot\mathbf{\Sigma}(\mathbf{D})\cdot\mathbf{J}^T = {\sigma_D}^2\mathbf{J}\cdot\mathbf{J}^T \tag{15}$$

where $\mathbf{J}$ is the 5-by-2(n+m) Jacobian matrix that collects the derivatives of the motion vector $\boldsymbol{\theta}$ with respect to the distances $D_{x,i}$, $D_{y,i}$, $D_{x,j}$ and $D_{y,j}$. In this paper the building height is assumed to be known, thus the Jacobian matrix does not contain derivatives with respect to $D_{z,i}$ and $D_{z,j}$. Moreover, $\mathbf{\Sigma(D)}$ is assumed to be a diagonal matrix with non-zero elements pairs to σ_{Dx}^2 and σ_{Dy}^2. The latter are here supposed to be equal (i.e. $\sigma_{Dx}^2 = \sigma_{Dy}^2 = \sigma_D^2$), as in the case of the square grid resolution that characterizes COSMO-SkyMed data. However, the procedure might be further generalized to account for a non-square grid resolution.

In line with the intentions of the paper, each rigid motion component is individually treated. To provide a priori estimations of the output uncertainties due to errors in PS positioning, conditions (i) and (ii) are applied (for their definitions see Section 3.1). The variances of rigid motion parameters caused by errors in the PS positioning result:

$$\sigma_P(v_{x,\mathrm{G}}) = 0; \qquad \sigma_P(v_{z,\mathrm{G}}) = 0; \tag{16}$$

$$\sigma_P^2(\phi_x) = \sigma_D^2\frac{\left(n\cos^4\alpha_a + m\cos^4\alpha_d\right)}{\rho_y^2\left(n\cos^2\alpha_a + m\cos^2\alpha_d\right)^2}{\phi_x}^2; \quad \sigma_P^2(\phi_z) = \sigma_D^2\frac{\left(n\sin^4\alpha_a + m\sin^4\alpha_d\right)}{\rho_y^2\left(n\sin^2\alpha_a + m\sin^2\alpha_d\right)^2}{\phi_z}^2; \tag{17}$$

$$\sigma_P^2(\phi_y) = \sigma_D^2\frac{\rho_x^2\left(n\cos^4\alpha_a + m\cos^4\alpha_d\right) + D_z^2\left(n\sin^2\alpha_a\cos^2\alpha_a + m\sin^2\alpha_d\cos^2\alpha_d\right)}{\left[\rho_x^2\left(n\cos^2\alpha_a + m\cos^2\alpha_d\right) + D_z^2\left(n\sin^2\alpha_a + m\sin^2\alpha_d\right)\right]^2}{\phi_y}^2 \tag{18}$$

Note that, as expected, displacements turn out to be singularly not affected by errors in the PS positioning. Indeed,

if a pure vertical or horizontal translation occurs, the position of PSs is irrelevant in the estimation of the corresponding (i.e. vertical or horizontal) displacement. On the other hand, the variances of the estimated rotations are strictly dependent on satellite acquisition geometries (α_a , α_d), DInSAR resolution (σ_D), number of PSs (m, n) and building geometry (ρ_x, ρ_y and D_z).

4. Numerical simulations of uncertainties in results

Numerical simulations designed to assess the analytical expressions of Section 3 are herein presented. The core idea of the procedure is to impose a rigid motion to a building, simulate SAR data, corrupt them by introducing measurement and PS positioning uncertainties, and re-estimate the motion parameters according to Eq. (4). To statistically characterize results, Monte Carlo simulations are performed, and mean values and standard deviations of the estimated motion parameters are assessed. Then, numerically estimated uncertainties are compared to those obtained by means of Eqs. (8,9,13,14) and Eqs. (16-18). With more details, the case study consists in a 15 m tall building featured by a flat roof and a 24x36 m rectangular plan, inclined by 20° relative to the west-east direction. The incidence angles of ascending and descending satellite orbits are assumed equal to α_a = 30° and α_d = 25°, respectively. Number of PSs in ascending and descending orbits are, respectively, n = 60 and m = 40.

The analysis is repeated 1000 times, each with randomly extracted values to simulate displacement measurement and positioning uncertainties. Uncertainties in PS positioning are related to the characteristic spatial resolution of SAR images, which does not enable the exact position of PSs to be known. Dealing with COSMO-SkyMed data, the spatial resolution is about 3 m, implying that the building surface is ideally subdivided into a 3x3 m grid. At most one PS is identifiable in each grid cell, with the concrete possibility that no PS is detected in certain cells. To account for this source of uncertainty, PSs are initially placed at random positions inside the 3x3 m grid (green dots in Fig. 2a). In real applications, one can detect the presence of a PS in a cell but not its exact location inside it, implying that the green dots of Fig. 2a are actually unknowns. In the absence of more accurate information, the typical procedure is that of allocating the PS to the relative cell center point, as represented in Fig. 2b. Then, the PS coordinates in terms of latitude and longitude are truncated to the fifth digital place, corresponding to a resolution of 0.8 m (see Fig. 2c). Aiming at the characterization of the result variability due to positioning uncertainties, Monte Carlo simulations are carried out by randomly extracting n+m PSs on the building. Conceived as such, Monte Carlo analyses also allow to define the not yet explored σ_D , statistically characterizing the discrepancy between exact and actually used PS positions (green and red markers of Fig. 2, respectively). Such distances present values in the range [-1.9;1.9] m, mainly concentrated around 0 m. Distances are modelled as a Gaussian-like distribution having a standard deviation σ_D of 0.9 m. Then, the LOS displacement in ascending orbit $d_{a,i}$ of each PS is computed by considering the imposed building rigid motion and the PSs exact position (see Eqs. 1-2). Finally, the thus obtained ascending LOS displacements are attributed to the actually used PSs position to derive the building motion affected by PS positioning errors (see Eq. 4). The same procedure is applied also for the descending LOS displacements $d_{d,i}$.

Finally, the noise-corrupted LOS displacement is obtained by adding a random noise to each measure. The noise is randomly extracted from a normal distribution, with standard deviation σ_H = 2 mm/yr.

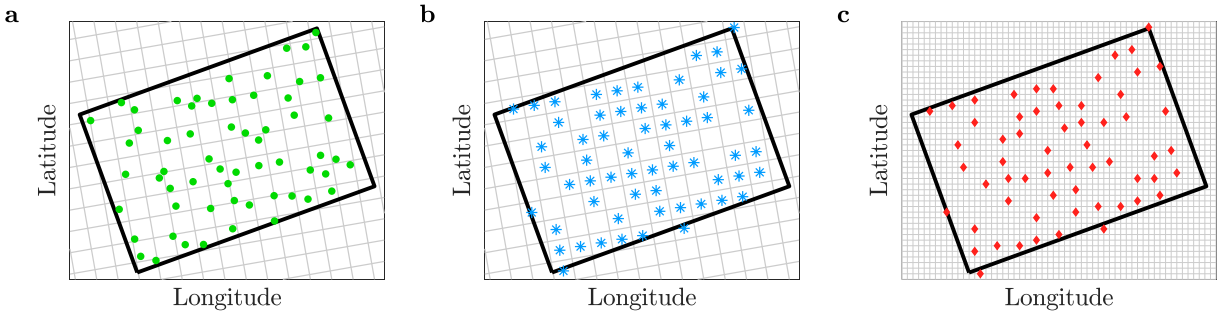

Fig. 2. Positioning simulation of n=60 PSs along the ascending orbit: (a) random locations, (b) cell centers allocation, (c) latitude and longitude coordinates truncation.

5. Results and discussion

For each imposed motion component, numerical uncertainties obtained as illustrated in Section 4 are compared to those analytically derived. For discussion purposes, the case of a specific imposed motion $\boldsymbol{\theta}$ =[$v_{x,G}$ = 10 mm, $v_{z,G}$ = 50 mm, ϕ_x = 2 mrad, ϕ_y = 0 mrad, ϕ_z = 1 mrad] is presented, with "mrad" denoting milliradians. The comparison, reported in Table 1 (where θ_k represents a generic motion component), shows a good agreement between analytical and numerical results, especially with regard to imposed motion parameters and estimated ones (average of simulations affected by both errors). Numerical measurement uncertainties $\sigma_M(\theta_k)$ are fairly consistent with the analytical values, while significant differences are obtained between numerical and analytical positioning uncertainties $\sigma_P(\theta_k)$. Indeed, analytical variances of $v_{x,G}$ and $v_{z,G}$ related to positioning errors are equal to zero according to Eq. (16), whereas numerical results return $\sigma_P(\theta_k)$ values having the same magnitude of $\sigma_M(\theta_k)$. To explain such discrepancies, the assumption of uncorrelated motion components is to be checked. The correlation matrices $\mathbf{R}_M(\boldsymbol{\theta})$ and $\mathbf{R}_P(\boldsymbol{\theta})$ of the 1000 numerical estimations read:

$$\mathbf{R}_M(\boldsymbol{\theta}) = \begin{bmatrix} 1.00 & 0.19 & -0.14 & -0.63 & 0.01 \\ 0.19 & 1.00 & 0.02 & 0.01 & -0.02 \\ -0.14 & 0.02 & 1.00 & 0.22 & -0.26 \\ -0.63 & 0.01 & 0.22 & 1.00 & 0.01 \\ 0.01 & -0.02 & -0.26 & 0.01 & 1.00 \end{bmatrix}; \quad \mathbf{R}_P(\boldsymbol{\theta}) = \begin{bmatrix} 1.00 & 0.71 & -0.08 & -0.58 & -0.02 \\ 0.71 & 1.00 & 0.03 & 0.01 & -0.02 \\ -0.08 & 0.03 & 1.00 & 0.21 & -0.86 \\ -0.58 & 0.01 & 0.21 & 1.00 & -0.02 \\ -0.02 & -0.02 & -0.86 & -0.02 & 1.00 \end{bmatrix} \quad (19)$$

where the sequence of variables is as follows: $v_{x,G}$, $v_{z,G}$, ϕ_x, ϕ_y and ϕ_z. Eq.(19) shows that the correlation among motion components is not actually negligible, as correlation matrices are not diagonal. In particular, $v_{x,G}$ and ϕ_y are highly correlated in terms of displacement measurement errors, while PS positioning uncertainties lead to correlations among $v_{x,G}$, $v_{z,G}$ and ϕ_y as well as among ϕ_x and ϕ_z. Such correlations also explain the results of Fig. 3, where displacement measurement and PS positioning uncertainties (both analytical and numerical), together with the total uncertainty, are presented for imposed motion parameters varying in the ranges: $v_{x,G} \in [0;15]$ mm, $v_{z,G} \in [0;75]$ mm, $\phi_x \in [0;3]$ mrad, $\phi_y \in [0;3]$ mrad, $\phi_z \in [0;1.5]$ mrad.

Table 1. Comparison between analytical and numerical results.

		$v_{x,G}$ [mm]	$v_{z,G}$ [mm]	ϕ_x [mrad]	ϕ_y [mrad]	ϕ_z [mrad]
θ_k	Imposed	10.00	50.00	2.00	0	1.00
	Simulation (mean value)	9.97	49.99	1.97	0.01	0.96
$\sigma_M(\theta_k)$	Simulation	0.425	0.227	0.031	0.018	0.057
	Eqs. (8,9,13,14)	0.573	0.235	0.033	0.023	0.061
$\sigma_P(\theta_k)$	Simulation	0	0	0.024	0	0.020
	Eqs. (16-18).	0.478	0.178	0.025	0.022	0.048

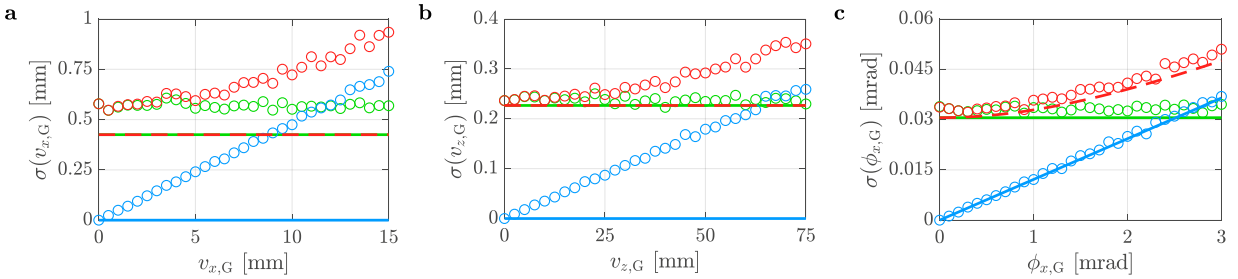

Fig. 3. Analytical (solid lines) and numerical (circular markers) uncertainties: displacement measurements in green, PS positioning in blue, both contributions in red

As regards $v_{x,G}$, its correlation with the other motion components is significant in both the uncertainty evaluations, thus analytical and numerical estimations differ both for measurement and PS positioning uncertainties (Fig. 3a). On the other hand, $v_{z,G}$ is correlated with the other motion components only when dealing with PS positioning errors, thus analytical and numerical results are slightly different in one case but almost coinciding in the other (Fig. 3b). The same does not happen for ϕ_x: despite its non-negligible correlation with ϕ_z, it presents an almost perfect agreement between analytical and numerical results (Fig. 3c). This is probably due to the low ϕ_z values considered in the performed numerical simulations, which makes the effect of the correlation between ϕ_x and ϕ_z irrelevant.

6. Conclusions

This paper investigates the potential of the DInSAR technologies for the structural monitoring of isolated buildings. Although the availability of high-resolution data from recently developed SAR constellations has paved the way for the satellite monitoring of single structures or infrastructures, its reliability assessment is still challenging. Within this framework, the present paper proposes a procedure for estimating the rigid motion of isolated buildings from SAR data, as well as analytical expressions for evaluating the uncertainties of the estimated motion components. This allows to perceive in advance whether the use of DInSAR techniques is appropriate for a certain case study. Indeed, knowing the order of magnitude of the minimum accuracy (i.e. maximum uncertainty) required to detect the expected rigid motion, analytical expressions might be used in reverse to calculate the necessary number of PSs (n+m). Finally, the latter compared to the maximal amount of detectable PSs (i.e. ratio of building plan to grid cell area) could be used as an indicator of the application reasonableness. Analytical expressions proposed in this paper are verified against results deriving from numerical simulations, performed accounting for the displacement measurement and PS positioning uncertainties that unavoidably affect SAR data. Discrepancies between numerical and analytical results are explained as due to the assumption of uncorrelated motion components. However, presented results demonstrate the potential of the DInSAR-based structural monitoring, as well as the need to analytically characterize the motion parameter uncertainties without the assumption of uncorrelated movements.

Acknowledgements

This research was supported by the ReLUIS-DPC 2019-2021 Project (Line WP6) and the FAR Mission Oriented 2021 Project (Satellite Methods for Structural Monitoring, SM4SM). The financial support of DPC, Reluis Consortium, UNIMORE and “Fondazione di Modena” is gratefully acknowledged.

References

Barreca, G., Bruno, V., Cocorullo, C., Cultrera, F., Ferranti, L., Guglielmino, F., Guzzetta, L., Mattia, M., Monaco, C., Pepe, F., 2014. Geodetic and geological evidence of active tectonics in south-western Sicily (Italy). Journal of Geodynamics 82, 138–149.

Bianchini, S., Pratesi, F., Nolesini, T., Casagli, N., 2015. Building Deformation Assessment by Means of Persistent Scatterer Interferometry Analysis on a Landslide-Affected Area: The Volterra (Italy) Case Study. Remote Sensing 7(4), 4678–4701.

Calò, F., Ardizzone, F., Castaldo, R., Lollino, P., Tizzani, P., Guzzetti, F., Lanari, R., Angeli, M. G., Pontoni, F., Manunta, M., 2014. Enhanced landslide investigations through advanced DInSAR techniques: The Ivancich case study, Assisi, Italy. Remote Sensing of Environment 142, 69–82.

Cavalagli, N., Kita, A., Falco, S., Trillo, F., Costantini, M., Ubertini, F., 2019. Satellite radar interferometry and in-situ measurements for static monitoring of historical monuments: The case of Gubbio, Italy. Remote Sensing of Environment 235, 111453.

Milillo, P., Giardina, G., Perissin, D., Milillo, G., Coletta, A., Terranova, C., 2019. Pre-collapse space geodetic observations of critical infrastructure: The Morandi Bridge, Genoa, Italy. Remote Sensing 11(12), 1403.

Noviello, C., Peduto, D., Verde, S., Zamparelli, V., Fornaro, G., Pauciullo, A., Reale, D., Nicodemo, G., Ferlisi, S., Gulla, G., 2020. Monitoring Buildings at Landslide Risk With SAR: A Methodology Based on the Use of Multipass Interferometric Data. IEEE Geoscience and Remote Sensing Magazine 8(1), 91–119.

Reale, D., Fornaro, G., Pauciullo, A., Zhu, X., Bamler, R., 2011. Tomographic imaging and monitoring of buildings with very high resolution SAR data. IEEE Geoscience and Remote Sensing Letters 8(4), 661–665.

Talledo, D. A., Miano, A., Bonano, M., di Carlo, F., Lanari, R., Manunta, M., Meda, A., Mele, A., Prota, A., Saetta, A., Stella, A., 2022. Satellite radar interferometry: Potential and limitations for structural assessment and monitoring. Journal of Building Engineering 46, 103756.